Research Square

Preprints are preliminary reports that have not undergone peer review.
They should not be considered conclusive, used to inform clinical practice,
or referenced by the media as validated information.

Dysregulated Cytosolic Redox Homeostasis in Patient-Derived Takotsubo Syndrome Cardiomyocytes

Vikram Vamsi Priya
Universitätsmedizin Göttingen
Wiebke Maurer
Universitätsmedizin Göttingen
Aylin Anna Seedorf
Universitätsmedizin Göttingen
Juan Camilo Cárdenas-Arciniegas
Universitätsmedizin Göttingen
Annette Hillemann
Universitätsmedizin Göttingen
Katrin Streckfuss-Bömeke
University of Würzburg
Dörthe Magdalena Katschinski
doerthe.katschinski@med.uni-goettingen.de

Universitätsmedizin Göttingen

Research Article

Keywords: Takotsubo syndrome, induced pluripotent stem cell-derived cardiomyocytes, redox homeostasis, glutathione, lipid peroxidation, 4-hydroxynonenal

Posted Date: November 18th, 2026

DOI: https://doi.org/10.21203/rs.3.rs-11573870/v1

License: This work is licensed under a Creative Commons Attribution 4.0 International License.
Read Full License

Additional Declarations: No competing interests reported.

Abstract

Takotsubo syndrome (TTS) is an acute stress-associated heart failure syndrome in which catecholamine excess is thought to interact with an intrinsic myocardial vulnerability. Oxidative stress has been implicated in its pathophysiology, but the underlying redox alterations in patient-derived cardiomyocytes remain poorly defined. We therefore investigated basal redox and metabolic homeostasis in induced pluripotent stem cell-derived cardiomyocytes from two TTS patients and two control lines. Cytosolic and mitochondrial H_2O_2-sensitive HyPer7 signals, glutathione redox potential (E_{GSH}), total NADP/NADPH abundance, ATP content, and 4-hydroxynonenal were assessed under unstimulated conditions. Basal HyPer7 ratios were not consistently altered in the TTS lines. In contrast, cytosolic E_{GSH} was altered in both TTS lines, although in opposite directions. TTS5 showed more reducing E_{GSH}, along with reduced ATP and increased lipid peroxidation, whereas TTS8 showed more oxidized E_{GSH} with largely preserved metabolic and lipid-peroxidation parameters. These findings indicate that TTS cardiomyocytes exhibit intrinsic but heterogeneous disturbances in cytosolic redox conditions. Patient-specific differences in how redox balance, metabolism, and oxidative damage interact may contribute to individual susceptibility to stress-induced myocardial dysfunction. These findings identify disturbed coordination of cytosolic redox homeostasis and cellular metabolism as an intrinsic feature of patient-derived TTS cardiomyocytes that may contribute to susceptibility to acute stress-induced myocardial dysfunction.

Introduction

Takotsubo syndrome (TTS), also referred to as stress cardiomyopathy, is an acute heart failure syndrome characterized by transient regional ventricular dysfunction extending beyond a single coronary territory [6]. Patients commonly present with chest pain, dyspnoea, electrocardiographic changes, and elevated cardiac biomarkers, thereby mimicking acute myocardial infarction; however, the extent of ventricular dysfunction cannot be explained by obstructive coronary artery disease [26]. Although the classical phenotype involves apical akinesia or dyskinesia with basal hypercontractility, midventricular, basal, and focal variants are increasingly recognized [24]. TTS predominantly affects postmenopausal women and is often preceded by emotional or physical stress, although a trigger is not mandatory. Despite typically rapid recovery of left ventricular function, TTS is associated with substantial acute morbidity, including heart failure, arrhythmias, thromboembolic events, and cardiogenic shock [6].

The pathophysiology of TTS is incompletely understood and likely multifactorial [15, 16, 18]. Excessive sympathetic activation and acute catecholamine surges are widely considered key initiating factors [10]. Proposed downstream mechanisms include altered β-adrenergic signaling, intracellular Ca^{2+} overload, energy deficit, systemic and myocardial inflammation, endothelial impairment, and metabolic dysregulation, most of which have been established in mouse models [7, 19, 20]. Evidence from patient-specific induced pluripotent stem cell-derived ventricular cardiomyocytes (iPSC-CMs) suggests an intrinsic myocardial susceptibility, characterized by exaggerated β-adrenergic responses, impaired contractility, and altered electrophysiological and metabolic properties following catecholamine exposure [3]. An atrial cardiac stem cell model of the same TTS patients supports a mechanistic link

between genetic predisposition to an excessive catecholaminergic stress response, dysregulated phosphodiesterase (PDE) signaling, and atrial arrhythmogenesis, identifying PDE4 as a potential therapeutic target in TTS [4]. These observations support a model in which an acute neurohumoral stress response interacts with a pre-existing, patient-specific vulnerability.

Among the proposed mechanisms for intrinsic vulnerability, oxidative stress has emerged as another potential link between catecholamine excess and myocardial dysfunction, supported by myocardial dihydroethidiume (DHE) staining, elevated malondialdehyde levels, and reduced glutathione levels [11, 13]. Metabolomic analyses further suggest systemic metabolic remodeling and impaired cardiac energetics, including alterations in glucose and lipid metabolism, amino acid pathways, and glutathione-related processes [7, 25]. Catecholamines can promote ROS generation through catecholamine auto-oxidation, β-adrenergic signaling, activation of NADPH oxidases, and mitochondrial ROS production [2]. Increased ROS can disrupt Ca^{2+} handling, oxidatively modify contractile and metabolic proteins, reduce nitric oxide bioavailability, and contribute to endothelial and microvascular dysfunction. Thus, catecholamine-induced redox imbalance may both contribute to and exacerbate myocardial stunning.

Importantly, oxidative stress cannot be adequately described by bulk ROS levels alone [21]. In particular, DHE-based staining provides limited subcellular information and lacks ROS specificity when based on total fluorescence because DHE can generate multiple fluorescent oxidation products that conventional microscopy cannot distinguish. Cellular redox homeostasis is compartmentalized and governed by the interplay between oxidant production, antioxidant capacity, and metabolic reducing equivalents [23]. The glutathione redox potential, E_{GSH}, reflects the balance between reduced and oxidized glutathione and complements hydrogen peroxide-sensitive probes [8, 22]. NADPH serves as a critical source of reducing equivalents for glutathione- and thioredoxin-dependent antioxidant systems, whereas ATP availability constrains glutathione synthesis and metabolic adaptation. Lipid peroxidation products such as 4-hydroxynonenal (4-HNE) further indicate oxidative membrane damage and can modify proteins involved in mitochondrial function, excitation–contraction coupling, and cellular metabolism. Integrating these parameters enables discrimination among increased oxidant production, impaired antioxidant defenses, and downstream oxidative damage.

It remains unknown whether TTS is characterized by a uniform redox phenotype or by patient-specific alterations in redox homeostasis. In the present study, we therefore quantified basal cytosolic and mitochondrial H_2O_2 levels, E_{GSH}, total NADP/NADPH abundance, ATP content, and 4-HNE in iPSC-CMs derived from TTS patients and matched controls. By focusing on unstimulated conditions, we aimed to identify intrinsic alterations in redox homeostasis and to define the relationship between glutathione redox balance, cellular energetics, and lipid peroxidation in TTS.

Materials and Methods

Human induced pluripotent stem cell lines

Four human induced pluripotent stem cell (hiPSC) lines were investigated: two control lines, WT4 and CTRL1 [1, 3], and two lines derived from patients with TTS, i.e., TTS5 and TTS8 [3], which were described earlier. The TTS patients used in this study are registered in the International Takotsubo Registry (NCT01947621). The cell lines were established in the Laboratory for Translational Stem Cell Research, Prof. Dr. Katrin Streckfuss-Bömeke, Department of Cardiology and Pneumology, University Medical Center Göttingen.

The study was conducted in accordance with the Declaration of Helsinki and approved by the local Ethics Committee of the University Medical Center Göttingen (Az-10/9/15) and the Ethics Committee of the University of Zürich (KEK-No.: 2013-0075). Informed consent was obtained from all subjects involved in the study.

Differentiation of hiPSCs into cardiomyocytes

Human iPSC lines were differentiated into ventricular CM by modulating WNT signaling, followed by metabolic selection, and were cultured for at least 60 days [5, 9]. Human iPSCs and the derived CM were cultured under feeder-free and serum-free conditions on a Geltrex matrix (354230, Th. Geyer, Germany) in a humidified incubator at 37°C and 5% CO_2. The iPSCs were passaged twice a week at a confluency of 70–80% and cultured in StemMACS iPS-Brew XF medium (130.104.368, Miltenyi Biotec, Germany) (TTS lines) with daily medium changes. The differentiation process was initiated at a confluency of 50–90%. Two weeks after starting CM differentiation, cells were replated and metabolically selected by lactate. The differentiated CM were cultured for 60 days with a Cardio Culture medium ((RPMI 1640 supplemented with GlutaMAX, HEPES (72400-054, Thermo Fisher Scientific), and B-27 Supplement (17504-044, Thermo Fisher Scientific)), changed twice a week and then passaged by treating them with trypsinization (0.25% trypsin/EDTA, 25200056, Thermo Fisher Scientific) at 37°C for 5 min. Afterward, the cells were seeded in Cardio Digest Medium (Cardio Culture medium supplemented with 20% FBS (10270106, Gibco) and 2 µM Thiazovivin (420220-10MG, Merck) allowed to settle for one day before the medium was changed back to Cardio Culture medium. Measurements were performed 5–7 days afterward, with changes to Cardio Culture medium made every 2–3 days. iPSC-derived CM were analyzed 8–12 weeks after the initiation of the differentiation process. The purity of the iPSC-CM was assessed via flow analysis, focusing on cardiac troponin T positivity (> 75% cardiac TNT+), as well as through qPCR (hOCT4, hMLC2v) and immunofluorescence (α-actinin and MLC2v) analysis of CM-specific markers.

Transient expression of genetically encoded redox sensors

Cytosolic and mitochondrial H_2O_2-sensitive signals were assessed using pCS2+-HyPer7-NES (Addgene, 136467) and pCS2+-HyPer7-MLS (Addgene, 136470), respectively. Cytosolic and mitochondrial E_{GSH} were assessed using pLPCX-cyto-Grx1-roGFP2 (Addgene, 64975) and pLPCX-mito-Grx1-roGFP2 (Addgene, 64977).

Cardiomyocytes were plated on to the Matrigel coated 10 mm or 18 mm coverslips in 24 well (150 x 10^3 cells) or 12 well plates (300 x 10^3 cells) and transiently transfected after 5–7 days of plating using ViaFect transfection reagent (Promega, E4982). Plasmid DNA and ViaFect were combined at a mass-to-volume ratio of 1:4 in Opti-MEM (GibCo, 31985-070). The transfection mixture was incubated for 40–50 min at room temperature and then added dropwise to the cultures. Measurements were performed 48 h after transfection.

Live-cell imaging conditions

Real-time cell imaging experiments were performed using an inverted epifluorescence microscope IX83 (Olympus) as described earlier [14]. The microscope is equipped with a super Apochromat 10x/0.40 dry objective and digital CMOS camera, ORCA-flash 4.0/ C11440 (Hamamatsu, Japan). An MT20 illumination system with a 150 W Xenon arc lamp was used for ratiometric imaging of HyPer7, utilizing excitation wavelengths of 405/20 nm and 485/20 nm. Emission was alternately collected using a motorized filter wheel equipped with the following filter combinations: beam splitter 420 (for HyPer low), 500 (for HyPer high), and emission filter 525/30 for both channels. For the HyPer ratio, the emission excited at the wavelength 500 nm was divided by the emission at 420 nm (500/420). The imaging interval was set to 120 sec. Data acquisition was carried out using the CellSens Dimension version 1.18 software (Olympus, Japan). All imaging experiments were performed on CM placed on coverslips that were fitted into the holding chamber, with the appropriate temperature and CO_2 levels for live cell imaging provided by the Cell VIVO incubation chamber (Pecon, Germany). Camera binning for real-time imaging was set to 4 × 4, light intensity was 3.95%, and exposure time was 1 s. After reaching stable baseline readings, recordings were continued for 20 min and at the end of each recording, 200 µmol/L H_2O_2 was added to confirm sensor responsiveness. Basal ratios were determined from the stable pre-stimulation period.

Measurement of cytosolic and mitochondrial E_{GSH}

The E_{GSH} was determined using cytosolic or mitochondrially targeted Grx1-roGFP2. Forty-eight hours after transfection, cells were imaged using the epifluorescence microscope described above, equipped with an LC-SOLASE-365 LED fluorescence excitation light source and sequential excitation at 378/52 and 500/20 nm with fluorescence emission collected at approximately 510 nm. Baseline ratios were recorded until stable, typically for approximately 10 min. Separate coverslips were exposed to 500 µmol/L H_2O_2 (Roth, 8070.2) to obtain the maximally oxidized sensor signal or to 10 mmol/L DTT (Roth, 6908.1) to obtain the maximally reduced signal. Imaging was continued for approximately 10 min or until the signal reached a plateau. The degree of sensor oxidation was calculated from the fluorescence intensities obtained under basal, fully reduced, and fully oxidized conditions as described earlier [22]. E_{GSH} was subsequently calculated using the Nernst equation:

$E_{GSH} = E°'roGFP2 - (RT/2F) \ln [(1 - OxDroGFP2)/OxDroGFP2]$

where $E°'_{roGFP2}$ is − 280 mV, R is the universal gas constant, T is the absolute temperature, and F is the Faraday constant.

Measurement of cellular ATP

Cellular ATP was assessed using BioTracker™ ATP-Red Live Cell Dye (Merck, SCT045). Cardiomyocytes (40 x 10^3 cells) were seeded onto Matrigel-coated 10-mm coverslips in 24-well plates and analyzed 5–7 days after replating. Cells were washed twice with Tyrode (1.8 mM $CaCl_2$, 10 mM glucose, 10 mM HEPES, 5.4 mM KCl, 2 mM $MgCl_2$, 140 mM NaCl) and incubated with 5 µmol/L ATP-Red dye (1:1000 dilution of the 5 mmol/L stock) for 15 min at 37°C. After incubation, cells were washed once and transferred to an imaging chamber containing fresh Tyrode solution. Bright-field and fluorescence images were acquired using a 20X objective. ATP-Red fluorescence was excited at 554/23 nm and detected using a Cy3 filter set. Ten randomly selected fields were acquired per coverslip using identical acquisition settings. Images were analyzed using Fiji/ImageJ. Background-corrected fluorescence intensity was quantified in randomly selected regions of interest. Identical image-processing parameters were applied to all experimental groups. The mean fluorescence intensity for each cell was used from each experimental replicate and is reported in arbitrary units.

Quantification of total NADP and NADPH

Total NADP and NADPH abundance was quantified using the NADP/NADPH-Glo™ assay kit (Promega, G9081) according to the manufacturer's instructions. Snap-frozen cardiomyocyte pellets were thawed on ice, centrifuged briefly at 13 000 × g, and resuspended in 200 µL phosphate-buffered saline. A standard curve ranging from 0 to 1000 nmol/L $NADP^+$ was prepared. Samples and standards were transferred to white 96-well plates in 50 µL aliquots, followed by 50 µL of freshly prepared detection reagent. Luminescence was recorded at 37°C using a CLARIOstar plate reader (BMG LabTech) at 5 min intervals for 60 min. Values recorded after 20 min were used for analysis. Standards and samples were measured in duplicate. Concentrations were derived from the $NADP^+$ standard curve and normalized to total protein content. Because the assay quantified the combined pyridine nucleotide pool, results are reported as total NADP/NADPH abundance.

Determination of total protein concentration

Protein concentrations were measured using the DC Protein Assay (Bio-Rad, 5000113) according to the manufacturer's instructions. Bovine serum albumin was used to generate the standard curve. Absorbance was measured at 750 nm, and protein concentrations were calculated by interpolation from the standard curve.

Quantification of intracellular 4-HNE adducts and extracellular 4-HNE

Lipid peroxidation was assessed by measuring intracellular 4-HNE–protein adducts and extracellular free 4-HNE. For extracellular 4-HNE measurements, conditioned culture medium was collected from replated cardiomyocytes. Intracellular 4-HNE adducts were measured in snap-frozen cell pellets. Cell pellets were lysed in 500 µL mild RIPA buffer containing 50 mmol/L Tris, 0.9% NaCl, and 0.1% sodium dodecyl sulfate, adjusted to pH 7.3. Lysates were mechanically homogenized and centrifuged at 5000 × g for 5 min at 4°C. The clarified supernatants were collected for analysis.

Free extracellular 4-HNE was measured using a 4-HNE ELISA kit (Abcam, ab287803). Intracellular 4-HNE adducts were quantified using the OxiSelect HNE Adduct Competitive ELISA kit (Cell Biolabs, STA-838). Assays were performed according to the manufacturers' instructions. The enzymatic reaction was stopped after color development in the upper standards, typically after 5–10 min, to avoid saturation. Absorbance was measured at 495 nm using a CLARIOstar (BMG) plate reader. Intracellular and extracellular 4-HNE values were normalized to total cellular protein content.

Statistical analysis

Statistical analyses were performed using GraphPad Prism version 10. Data are presented as individual data points with mean ± SEM. For comparisons between the four groups, ordinary one-way ANOVA followed by Tukey's multiple-comparisons test was used for normally distributed data. When multiple measurements originated from the same differentiation batch, nested one-way ANOVA followed by Tukey's multiple-comparisons test was employed to account for the hierarchical data structure. For data that did not meet the assumptions of parametric testing, the Kruskal-Wallis test followed by Dunn's multiple-comparisons test was used. Statistical significance was defined as a two-sided $P < 0.05$, and exact P values are reported where applicable.

Results

Basal H_2O_2-sensitive HyPer oxidation is not altered in TTS cardiomyocytes

To determine whether patient-derived TTS cardiomyocytes show intrinsic alterations in redox homeostasis under unstimulated conditions, we assessed basal cytosolic and mitochondrial HyPer ratios as a measure of H_2O_2-levels, compartment-specific E_{GSH}, total NADP/NADPH abundance, ATP content, and intracellular and secreted 4-HNE in two control and two TTS iPSC-CM lines. Basal cytosolic and mitochondrial HyPer ratios were broadly comparable among WT4, CTRL1, TTS5, and TTS8 (Fig. 1a and b). Although moderate variability was observed between individual lines, basal HyPer oxidation did not differ significantly between TTS and control lines in either the cytosol or mitochondria.

Cytosolic glutathione redox homeostasis is altered in both TTS lines

In contrast to the HyPer measurements, the cytosolic E_{GSH} was altered in both TTS lines (Fig. 1c). However, the direction of this shift differed markedly between the two lines. TTS5 displayed a significantly more negative cytosolic E_{GSH} than both control lines, indicating a more reducing cytosolic glutathione environment. Conversely, TTS8 showed a significantly less negative E_{GSH}, consistent with a more oxidized cytosolic glutathione state. Mitochondrial E_{GSH} showed only moderate line-to-line variation and no common TTS-associated alteration. These findings identify cytosolic, rather than mitochondrial, glutathione redox homeostasis as the principal compartment affected in both TTS lines, while demonstrating that the resulting redox state is patient-line specific.

Total NADP/NADPH abundance and ATP levels are selectively reduced in TTS5

Because maintaining the glutathione redox system depends on cellular reducing equivalents, we assessed total NADP/NADPH abundance (Fig. 2a). TTS5 showed the lowest mean total NADP/NADPH abundance and was significantly reduced compared with WT4, although it did not differ significantly from CTRL1. In contrast, TTS8 showed total NADP/NADPH abundance within the range of the control lines. Thus, reduced pyridine nucleotide abundance was detected in TTS5 relative to one control line but did not represent a shared feature of the two TTS lines. To determine whether the observed redox alterations were associated with changes in cellular energy status, ATP levels were quantified (Fig. 2b). ATP content was reduced in TTS5 compared with WT4, CTRL1, and TTS8. By contrast, ATP levels in TTS8 were preserved and remained within the control range. These findings indicate impaired basal cellular energetics in TTS5, whereas the oxidized cytosolic E_{GSH} of TTS8 was not accompanied by detectable ATP depletion.

Lipid peroxidation is enhanced in TTS5 but not in TTS8

To assess whether altered redox homeostasis was associated with oxidative membrane damage, intracellular 4-HNE adducts and extracellular 4-HNE secretion were measured (Fig. 3a and b). Intracellular 4-HNE adduct levels were increased in TTS5 compared with WT4, although the difference from CTRL1 was not significant. In addition, intracellular 4-HNE tended to be higher in TTS5 than in TTS8. The difference was more pronounced for extracellular 4-HNE. TTS5 showed significantly increased 4-HNE secretion compared with WT4, CTRL1, and TTS8. In contrast, TTS8 showed no increase in either intracellular 4-HNE adducts or extracellular 4-HNE secretion relative to the control lines. Thus, evidence of enhanced basal lipid peroxidation was restricted to TTS5.

Discussion

The present study analyzed intrinsic alterations in redox regulation in patient-derived TTS cardiomyocytes under unstimulated conditions. Both TTS lines showed abnormal cytosolic E_{GSH} despite no consistent increase in basal cytosolic or mitochondrial HyPer7 oxidation. However, the associated phenotypes differed (Fig. 4). TTS5 showed more reducing cytosolic E_{GSH}, reduced ATP, comparatively low total NADP/NADPH abundance, and increased intracellular and extracellular 4-HNE. In contrast,

TTS8 showed more oxidized cytosolic E_{GSH}, while ATP, pyridine nucleotide abundance, and lipid-peroxidation markers remained largely preserved. Thus, the shared feature was disturbed cytosolic redox regulation rather than a uniform increase in basal oxidation.

Evidence for oxidative stress in TTS has largely relied on indirect measurements, including DHE fluorescence in human myocardial biopsies [13] as well as DHE fluorescence and malonaldehyde levels in tissues from experimental models [27]. These approaches support altered oxidative status but do not resolve the responsible reactive species or their subcellular source. Our finding that basal HyPer7 oxidation was not increased in either TTS line therefore does not argue against redox involvement. HyPer7 and Grx1-roGFP2 report different aspects of redox biology: HyPer7 reflects local H_2O_2-sensitive probe oxidation, whereas Grx1-roGFP2 reports the glutathione redox state. Changes in glutathione synthesis, recycling, consumption, or compartmental handling may therefore alter E_{GSH} without producing a detectable change in steady-state HyPer7 ratios [17].

The opposing cytosolic E_{GSH} values in the two TTS lines suggest distinct adaptive states in resting cells. In TTS8, the more oxidized E_{GSH} was not accompanied by ATP depletion or increased 4-HNE, consistent with a likely compensated but potentially redox-vulnerable phenotype. In TTS5, by contrast, a more reducing cytosolic E_{GSH} coexisted with impaired energetics and lipid peroxidation. This apparently paradoxical combination may reflect compensatory maintenance of the glutathione pool during ongoing oxidative or electrophilic stress. A reducing E_{GSH} should therefore not be interpreted as evidence for the absence of oxidative damage. The TTS5 phenotype links lipid peroxidation to impaired cellular energetics. Increased 4-HNE, particularly in the extracellular fraction, was accompanied by reduced ATP and a comparatively small total NADP/NADPH pool. Lipid peroxidation may arise downstream of mitochondrial or enzymatic ROS generation, while 4-HNE can further modify mitochondrial, metabolic, ion-handling, and contractile proteins. These mechanisms could reinforce energetic dysfunction. However, the present data do not establish whether lipid peroxidation caused ATP depletion, whether impaired metabolism caused this depletion, or whether both developed in parallel from a common upstream defect.

The divergent phenotypes in the patient iPSC-derived cardiomyocytes are consistent with the clinical and mechanistic heterogeneity of TTS [6,12]. Catecholamine excess is thought to act on a variable background of myocardial, vascular, hormonal, and metabolic susceptibility. Patient-derived iPSC models may therefore reveal distinct cellular routes that converge on vulnerability to the same clinical syndrome [3]. In this framework, TTS5 represents a damage-associated phenotype with altered energetics and lipid peroxidation despite a reducing glutathione state, whereas TTS8 represents an oxidized but metabolically compensated phenotype. The common denominator is not uniform oxidation, but impaired coordination between cytosolic glutathione homeostasis, energy metabolism, and lipid detoxification. These findings raise the possibility that differences in basal redox homeostasis may represent an additional component of distinct intrinsic susceptibility. However, the present study is limited by the inclusion of only two TTS and two control iPSC lines, which limits how broadly these phenotypes can be

generalized to TTS as a whole. Moreover, differences in genetic background and other cell line-specific characteristics may contribute to the observed redox and metabolic differences and cannot be fully separated from disease-associated effects in the current experimental design. Whether the observed redox phenotypes influence catecholamine-dependent myocardial stress responses therefore remains to be investigated in larger panels of patient- and control-derived iPSC-CMs.

In conclusion, TTS cardiomyocytes showed abnormal cytosolic glutathione redox regulation without a consistent increase in basal H_2O_2-sensitive probe oxidation, although we analyzed only a limited number of iPSC lines. The two TTS lines displayed distinct redox-metabolic phenotypes, indicating that TTS-associated redox dysregulation is heterogeneous and cannot be described simply as increased basal ROS. Patient-specific differences in glutathione homeostasis, energy metabolism, and lipid-peroxidative damage may contribute to individual myocardial susceptibility.

Declarations

Competing interests

The authors have no relevant financial or non-financial interests to disclose. K.S.B. has no competing interests directly related to this work but has received grants from Novartis and Bayer and speaker honoraria from Novartis.

Ethics approval

The study was conducted in accordance with the Declaration of Helsinki and approved by the local Ethics Committee of the University Medical Center Göttingen (Az-10/9/15) and the Ethical Committee of the University of Zürich (KEK-No.: 2013-0075). Informed consent was obtained from all subjects involved in the study.

Funding

The project was financially supported by the German Research Foundation (Deutsche Forschungsgemeinschaft, DFG), Research Training Group 2824 (RTG 2824).

Author Contribution

V .V. P. and W.M. conceived, designed, performed the experiments, and analyzed data. A.A. S., J. C. A., and A. H. performed experiments. K. S.B. and D.M. K. acquired funding, designed and supervised experiments, analyzed data, and wrote the manuscript. All authors reviewed the manuscript

Acknowledgement

Vikram Vamsi Priya and Aylin Seedorf received fellowships from the Deutsche Forschungsgemeinschaft funded RTG 2824.

Data Availability

The data that support the findings of this study are available from the corresponding author upon justified request.

References

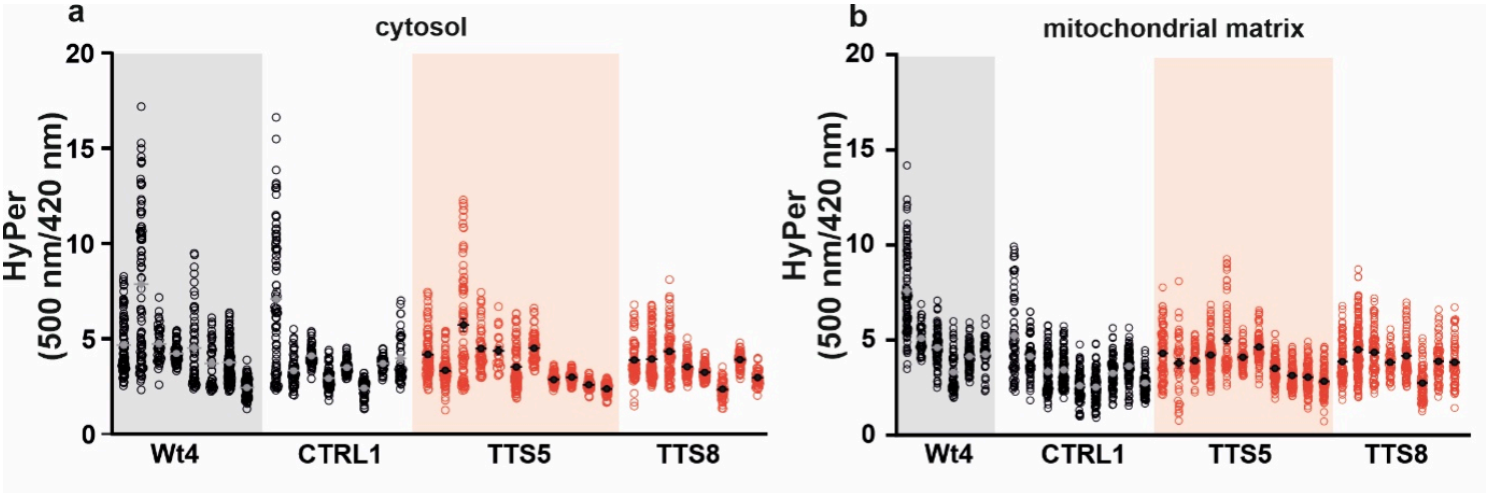
1. Bengel P, Dybkova N, Tirilomis P, Ahmad S, Hartmann N, B AM, Krekeler MC, Maurer W, Pabel S, Trum M, Mustroph J, Gummert J, Milting H, Wagner S, Ljubojevic-Holzer S, Toischer K, Maier LS, Hasenfuss G, Streckfuss-Bömeke K, Sossalla S (2021) Detrimental proarrhythmogenic interaction of Ca(2+)/calmodulin-dependent protein kinase II and Na(V)1.8 in heart failure. Nat Commun 12:6586. 10.1038/s41467-021-26690-1
2. Bleeke T, Zhang H, Madamanchi N, Patterson C, Faber JE (2004) Catecholamine-Induced Vascular Wall Growth Is Dependent on Generation of Reactive Oxygen Species. Circul Res 94:37–45. 10.1161/01.RES.0000109412.80157.7D
3. Borchert T, Hubscher D, Guessoum CI, Lam TD, Ghadri JR, Schellinger IN, Tiburcy M, Liaw NY, Li Y, Haas J, Sossalla S, Huber MA, Cyganek L, Jacobshagen C, Dressel R, Raaz U, Nikolaev VO, Guan K, Thiele H, Meder B, Wollnik B, Zimmermann WH, Luscher TF, Hasenfuss G, Templin C, Streckfuss-Bomeke K (2017) Catecholamine-Dependent beta-Adrenergic Signaling in a Pluripotent Stem Cell Model of Takotsubo Cardiomyopathy. J Am Coll Cardiol 70:975–991. 10.1016/j.jacc.2017.06.061
4. Brand C, Zinke C, Syed Ali G, Hubscher D, Ajmail K, Seedorf A, Steinker P, Treu F, Jung P, Eberl H, Li Y, Dybkova N, Feld L, Ghadri JR, Templin C, Sossalla S, Maack C, Voigt N, Nikolaev VO, Wollnik B, Streckfuss-Bomeke K (2026) Arrhythmic events and genetic variants as drivers for Takotsubo Syndrome: a patient-specific atrial stem-cell model. Signal Transduct Target Ther 11. 10.1038/s41392-026-03000-z
5. Burridge PW, Zambidis ET (2013) Highly efficient directed differentiation of human induced pluripotent stem cells into cardiomyocytes. Methods Mol Biol 997:149–161. 10.1007/978-1-62703-348-0_12
6. Ghadri J-R, Wittstein IS, Prasad A, Sharkey SW, Dote K, Akashi YJ, Camm AJ, Crea F, Lyon AR (2018) International expert consensus document on Takotsubo syndrome (Part I): clinical characteristics, diagnostic criteria, and pathophysiology. Eur Heart J 39:2032–2046. 10.1093/eurheartj/ehy076
7. Godsman N, Kohlhaas M, Nickel A, Cheyne L, Mingarelli M, Schweiger L, Hepburn C, Munts C, Welch A, Delibegovic M, Van Bilsen M, Maack C, Dawson DK (2022) Metabolic alterations in a rat model of takotsubo syndrome. Cardiovascular Res 118:1932–1946. 10.1093/cvr/cvab081

8. Gutscher M, Pauleau A-L, Marty L, Brach T, Wabnitz GH, Samstag Y, Meyer AJ, Dick TP (2008) Real-time imaging of the intracellular glutathione redox potential. Nat Methods 5:553–559. 10.1038/nmeth.1212
9. Lian X, Zhang J, Azarin SM, Zhu K, Hazeltine LB, Bao X, Hsiao C, Kamp TJ, Palecek SP (2013) Directed cardiomyocyte differentiation from human pluripotent stem cells by modulating Wnt/beta-catenin signaling under fully defined conditions. Nat Protoc 8:162–175. 10.1038/nprot.2012.150
10. Lyon AR, Bossone E, Schneider B, Sechtem U, Citro R, Underwood SR, Sheppard MN, Figtree GA, Parodi G, Akashi YJ, Ruschitzka F, Filippatos G, Mebazaa A, Templin C, Omerovic E (2016) Current state of knowledge on Takotsubo syndrome: a position statement from the Taskforce on Takotsubo Syndrome of the Heart Failure Association of the European Society of Cardiology. Eur J Heart Fail 18:8–27. 10.1002/ejhf.424
11. Lyon AR, Rees PSD, Prasad S, Poole-Wilson PA, Hardman SM, Yellon DM, Hausenloy DJ (2008) Stress (Takotsubo) cardiomyopathy–a novel pathophysiological hypothesis to explain catecholamine-induced acute myocardial stunning. Nat Clin Pract Cardiovasc Med 5:22–29. 10.1038/ncpcardio1066
12. McKenzie A, Bargout R (2025) Takotsubo Syndrome in 2025: Evolving Concepts in Pathophysiology, Diagnosis, and Long-Term Management. J Clin Med 15. 10.3390/jcm15010197
13. Münzel T, Templin C, Cammann VL, Hahad O (2021) Takotsubo Syndrome: Impact of endothelial dysfunction and oxidative stress. Free Radic Biol Med 169:216–223. 10.1016/j.freeradbiomed.2021.03.033
14. Nanadikar MS, Vergel Leon AM, Guo J, van Belle GJ, Jatho A, Philip ES, Brandner AF, Bockmann RA, Shi R, Zieseniss A, Siemssen CM, Dettmer K, Brodesser S, Schmidtendorf M, Lee J, Wu H, Furdui CM, Brandenburg S, Burgoyne JR, Bogeski I, Riemer J, Chowdhury A, Rehling P, Bruegmann T, Belousov VV, Katschinski DM (2023) IDH3gamma functions as a redox switch regulating mitochondrial energy metabolism and contractility in the heart. Nat Commun 14:2123. 10.1038/s41467-023-37744-x
15. Omerovic E, Citro R, Bossone E, Redfors B, Backs J, Bruns B, Ciccarelli M, Couch LS, Dawson D, Grassi G, Iacoviello M, Parodi G, Schneider B, Templin C, Ghadri JR, Thum T, Chioncel O, Tocchetti CG, van der Velden J, Heymans S, Lyon AR (2022) Pathophysiology of Takotsubo syndrome - a joint scientific statement from the Heart Failure Association Takotsubo Syndrome Study Group and Myocardial Function Working Group of the European Society of Cardiology - Part 1: overview and the central role for catecholamines and sympathetic nervous system. Eur J Heart Fail 24:257–273. 10.1002/ejhf.2400
16. Omerovic E, Redfors B (2022) Pathophysiology of Takotsubo syndrome - a joint scientific statement from the ESC/HFA. Eur J Heart Fail 24:274–281. 10.1002/ejhf.2439
17. Pak VV, Ezeriņa D, Lyublinskaya OG, Pedre B, Tyurin-Kuzmin PA, Mishina NM, Thauvin M, Young D, Wahni K, Martínez Gache SA, Demidovich AD, Ermakova YG, Maslova YD, Shokhina AG, Eroglu E, Bilan DS, Bogeski I, Michel T, Vriz S, Messens J, Belousov VV (2020) Ultrasensitive Genetically

Encoded Indicator for Hydrogen Peroxide Identifies Roles for the Oxidant in Cell Migration and Mitochondrial Function. Cell Metab 31:642–653e646. 10.1016/j.cmet.2020.02.003

18. Pelliccia F, Kaski JC, Crea F, Camici PG (2017) Pathophysiology of Takotsubo syndrome. Circulation 135:2426–2441. 10.1161/CIRCULATIONAHA.116.027121
19. Scally C, Abbas H, Ahearn T, Srinivasan J, Mezincescu A, Rudd A, Spath N, Yucel-Finn A, Yuecel R, Oldroyd K, Dospinescu C, Horgan G, Broadhurst P, Henning A, Newby DE, Semple S, Wilson HM, Dawson DK (2019) Myocardial and Systemic Inflammation in Acute Stress-Induced (Takotsubo) Cardiomyopathy. Circulation 139:1581–1592. 10.1161/CIRCULATIONAHA.118.037975
20. Shao Y, Redfors B, Ståhlman M, Täng MS, Miljanovic A, Möllmann H, Troidl C, Szardien S, Hamm C, Nef H, Borén J, Omerovic E (2013) A Mouse Model Reveals an Important Role for Catecholamine-Induced Lipotoxicity in the Pathogenesis of Stress-Induced Cardiomyopathy. Eur J Heart Fail 15:9–22. 10.1093/eurjhf/hfs161
21. Sies H, Belousov VV, Chandel NS, Davies MJ, Jones DP, Mann GE, Murphy MP, Yamamoto M, Winterbourn C (2022) Defining roles of specific reactive oxygen species (ROS) in cell biology and physiology. Nat Rev Mol Cell Biol 23:499–515. 10.1038/s41580-022-00456-z
22. Swain L, Kesemeyer A, Meyer-Roxlau S, Vettel C, Zieseniss A, Güntsch A, Jatho A, Becker A, Nanadikar MS, Morgan B, Dennerlein S, Shah AM, El-Armouche A, Nikolaev VO, Katschinski DM (2016) Redox Imaging Using Cardiac Myocyte-Specific Transgenic Biosensor Mice. Circ Res 119:1004–1016. 10.1161/circresaha.116.309551
23. Swain L, Nanadikar MS, Borowik S, Zieseniss A, Katschinski DM (2018) Transgenic Organisms Meet Redox Bioimaging: One Step Closer to Physiology. Antioxid Redox Signal 29:603–612. 10.1089/ars.2017.7469
24. Tsuchihashi K, Ueshima K, Uchida T, Oh-mura N, Kimura K, Owa M, Yoshiyama M, Miyazaki S, Haze K, Ogawa H, Honda T, Hase M, Hori M, Kodama K (2001) Transient left ventricular apical ballooning without coronary artery stenosis: a novel heart syndrome mimicking acute myocardial infarction. J Am Coll Cardiol 38:11–18. 10.1016/S0735-1097(01)01316-X
25. Vanni D, Viceconte N, Petrella G, Biccirè FG, Pelliccia F, Tanzilli G, Cicero DO (2021) A Pilot Study on the (1)H-NMR Serum Metabolic Profile of Takotsubo Patients Reveals Systemic Response to Oxidative Stress. Antioxid (Basel) 10. 10.3390/antiox10121982
26. Y-Hassan S, Tornvall P (2018) Epidemiology, pathogenesis, and management of takotsubo syndrome. Clin Cardiol 41:177–182. 10.1002/clc.22829
27. Zhang Z, Jin S, Teng X, Duan X, Chen Y, Wu Y (2017) Hydrogen sulfide attenuates cardiac injury in takotsubo cardiomyopathy by alleviating oxidative stress. Nitric Oxide 67:10–25. 10.1016/j.niox.2017.04.010

Figures



c

	wt		TTS	
E_{GSH}	Wt4	CTRL1	TTS5	TTS8
cytosol	-305.4 ± 0.9 mV (6) a	-306.3 ± 0.7 mV (6) a	-314.6 ± 1.4 mV (6) a,b	-289.4 ± 1.4 mV (6) a,b
mit. matrix	-288.2 ± 1.3 mV (6)	-286.6 ± 1.6 mV (6)	-290.7 ± 1.5 mV (6)	-285.1 ± 2.8 mV (6)

Figure 1

Basal cytosolic and mitochondrial redox parameters in control and Takotsubo syndrome (TTS) iPSC-derived cardiomyocytes.

Basal HyPer7 fluorescence ratios were measured in the cytosol (**a**) and mitochondrial matrix (**b**) of cardiomyocytes derived from two control lines (WT4 and CTRL1) and two Takotsubo syndrome lines (TTS5 and TTS8). HyPer7 ratios are expressed as the fluorescence emission ratio following excitation at 500 nm and 420 nm. Each data point represents one given cell; each sub-column represents one differentiation batch. Highlighted dots represent the mean +/- SEM. Data were analyzed using nested one-way ANOVA followed by Tukey's multiple comparison test. (**c**) Cytosolic and mitochondrial glutathione redox potentials (E_{GSH}) were determined using compartment-targeted Grx1-roGFP2. Statistical analysis was performed using an ordinary one-way ANOVA followed by Tukey's multiple comparison test. Data are presented as mean ± SEM, with the number of independent differentiations indicated in parentheses. Matched superscript letters denote statistically significant differences between groups.

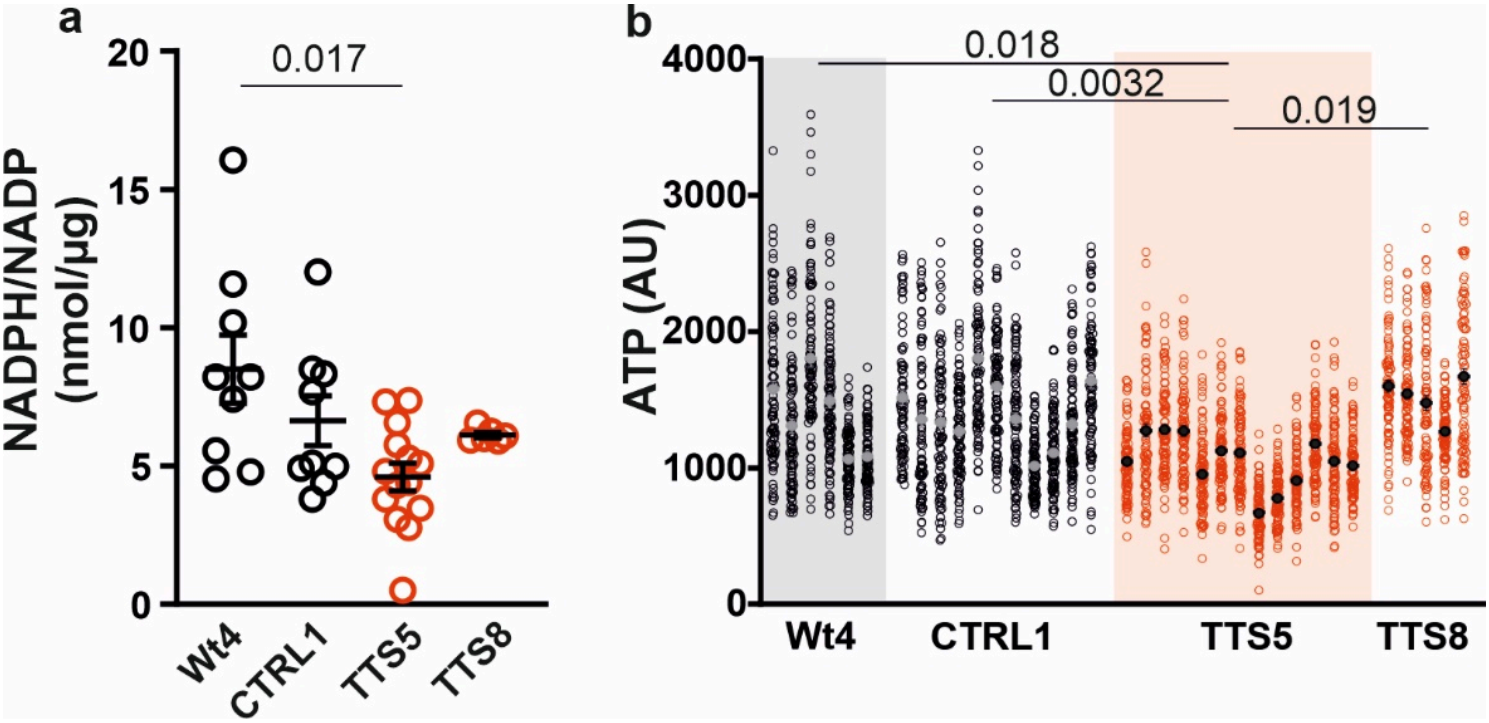


Figure 2

Total pyridine nucleotide abundance and ATP levels in control and Takotsubo syndrome (TTS) iPSC-derived cardiomyocytes.

(**a**) Total NADP/NADPH abundance was quantified in cardiomyocytes derived from two control lines (WT4 and CTRL1) and two Takotsubo syndrome lines (TTS5 and TTS8) and normalized to total protein content. Statistical analysis was performed using a Kruskal-Wallis test and Dunn ‘s multiple comparison test. Values are presented as mean ± SEM. (**b**) Cellular ATP levels were determined using ATP-Red fluorescence and are presented in arbitrary units (AU). Each data point represents one given cell; each sub-column represents one differentiation batch. Highlighted dots represent the mean +/- SEM. Data were analyzed using nested one-way ANOVA followed by Tukey’s multiple comparison test. Exact p-values are shown for statistically significant pairwise comparisons.

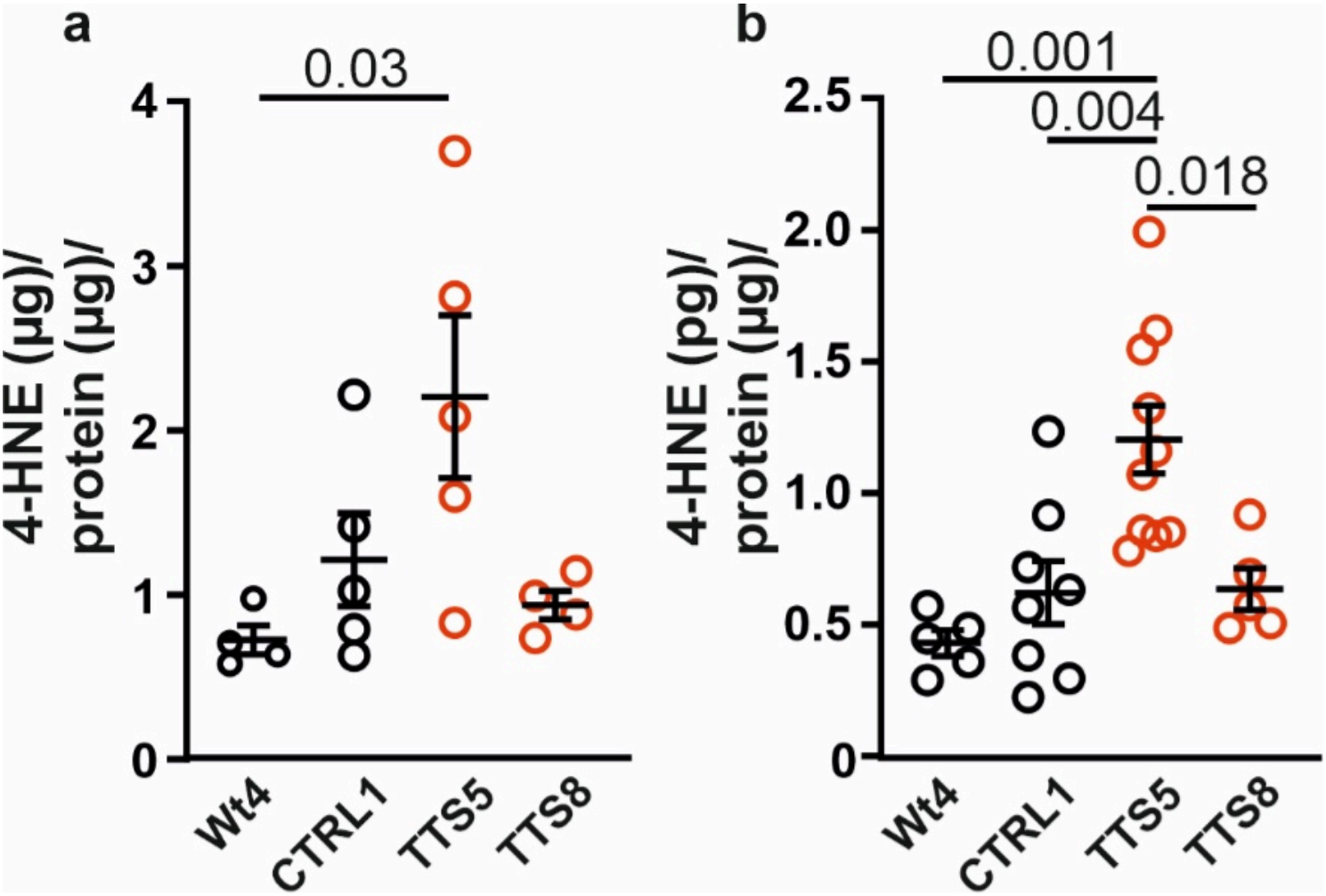


Figure 3

Intracellular 4-HNE adduct formation and extracellular 4-HNE levels in control and Takotsubo syndrome (TTS) iPSC-derived cardiomyocytes.

(**a**) Intracellular 4-hydroxynonenal (4-HNE)–protein adducts were quantified in cell lysates from two control lines (WT4 and CTRL1) and two Takotsubo syndrome lines (TTS5 and TTS8) using a competitive ELISA. (**b**) Free 4-HNE was measured in conditioned culture medium as an indicator of extracellular 4-HNE release. Intracellular and extracellular 4-HNE values were normalized to total cellular protein. Each data point represents a measurement in an independent cardiomyocyte differentiation batch, and statistical analysis was performed using a parametric one-way ANOVA followed by Tukey's multiple comparison. Data are presented as mean ± SEM. Exact p-values are shown for the indicated pairwise comparisons.

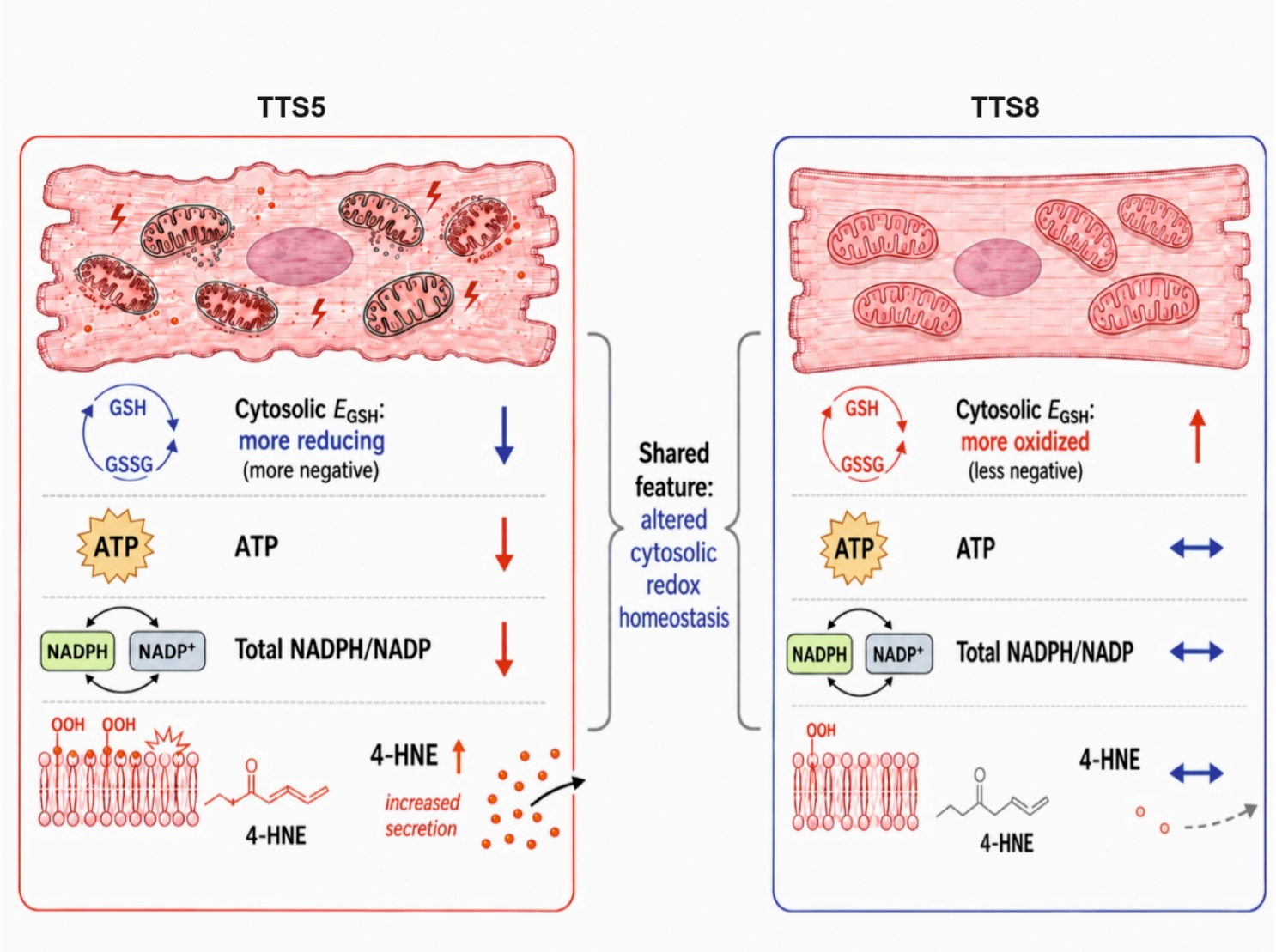


Figure 4

Distinct basal redox metabolic phenotypes in patient-derived Takotsubo syndrome (TTS) cardiomyocytes.

Schematic summary of the phenotypes observed in the two TTS iPSC-derived cardiomyocyte lines under basal conditions. The left panel (TTS5) shows a more reducing cytosolic glutathione redox potential (E_{GSH}), decreased ATP levels, reduced total NADP/NADPH abundance, and increased 4-hydroxynonenal (4-HNE), including enhanced extracellular release. The right panel (TTS8) depicts a phenotype with a more oxidized cytosolic E_{GSH}, while ATP, total NADP/NADPH abundance, and 4-HNE levels remain largely preserved. The central annotation indicates a shared feature: altered cytosolic redox homeostasis despite divergent metabolic and lipid-peroxidative consequences. Downward arrows (blue) indicate decreased values, upward arrows (red) indicate increased values, and horizontal arrows (blue) indicate no major change relative to control cardiomyocytes.